京都大学
KYOTO UNIVERSITY

Title	Differential roles of cyclin-dependent kinase 5 in tangential and radial migration of cerebellar granule cells.
Author(s)	Umeshima, Hiroki; Kengaku, Mineko
Citation	Molecular and cellular neurosciences (2012), 52: 62-72
Issue Date	2012-09-08
URL	http://hdl.handle.net/2433/166084
Right	© 2012 Elsevier Inc.
Type	Journal Article
Textversion	author

Differential roles of cyclin-dependent kinase 5 in tangential and radial migration of cerebellar granule cells

Hiroki Umeshima[a, b,*] and Mineko Kengaku[a, b, c]

[a] Institute for Integrated Cell-Material Sciences (WPI-iCeMS), Kyoto University, Yoshida-Honmachi, Sakyo-ku, Kyoto 606-8501, Japan

[b] Laboratory for Neural Cell Polarity, RIKEN, Brain Science Institute, Wako, Saitama 351-0198, Japan

[c] Graduate School of Biostudies, Kyoto University, Yoshida-Honmachi, Sakyo-ku, Kyoto 606-8501, Japan

[*] To whom correspondence should be addressed (e-mail: umeshima@icems.kyoto-u.ac.jp)

phone; 81-75-753-9832 fax; 81-75-753-9820

Editorial correspondence should be addressed to M.K. (e-mail: kengaku@icems.kyoto-u.ac.jp)

<u>Abstract</u>

The cerebellar granule cell is a unique neuron which undergoes tangential migration along axonal tracts and radial migration along glial fibers sequentially during postnatal development. Little is known about molecular bases of the differential kinetics of tangential and radial migration. Here we developed a time-lapse imaging assay for tangential migration of cerebellar granule cells, and investigated comparative contributions of cyclin-dependent kinase 5 (CDK5), a key regulator of neuronal migration, in tangential and radial migration of granule cells in vivo and in organotypic cultures. Overexpression of a dominant-negative form of CDK5 severely disrupted cell morphology and somal movement during radial migration, while it only moderately affected tangential migration. Dominant-negative inhibition of CDK5 induced formation of ectopic radial processes in granule cells in vivo which aberrantly elongated into the white matter in the cerebellum. Live imaging of granule cell migration in cerebellar slices revealed that CDK5 regulates not only nuclear migration but also centrosome movement during radial migration. These findings suggest a mode-specific function of CDK5 in neuronal migration.

Keywords: neuron, development, cerebellum, live cell imaging, centrosome

<u>Introduction</u>

Neuronal migration is a fundamental step during development of the mammalian central nervous system. Post-mitotic neurons migrate from their birthplace to their final destination for integration into specific neural circuits. Defects in neuronal migration cause a wide variety of brain diseases. CNS neuronal migration has been classified into two distinct phases, radial and tangential, by their direction of travel. Radial migration, as seen in a subset of cortical pyramidal cells, is the main mechanism for lamination of the cortex in which neurons move along the radial dimension of the neuroepithelium. The leading processes of radially migrating neurons often interact with radial fibers of glia. In contrast, tangential migration are seen in many interneurons traveling long distance from one brain region to another. Tangentially migrating neurons extend the leading processes parallel to the brain surface along axons of other neurons. These two phases of migrations usually take place in distinct cell types, in distinct microenvironments.

Cerebellar granule cells provide a unique opportunity to observe both radial and tangential migration in the same cells (Rakic, 1990; Komuro and Rakic, 1998; Komuro et al., 2001). During postnatal development of the cerebellum, granule cells immigrate from the external granular layer (EGL) to the internal granular layer (IGL).

Granule cells first elongate bipolar processes along the preformed parallel fiber axons of early-born granule cells and migrate tangentially along the longitudinal axis of cerebellar laminae. After the tangential migration, they make a vertical turn and then migrate radially along Bergmann glial fibers until they reach the IGL. We have previously shown that tangential and radial migration of granule cells exhibit different kinetics guided by leading processes with different morphological and molecular properties (Kawaji et al., 2004). However, little is known about the molecular mechanisms for driving the different kinetics of tangential and radial migration.

CDK5 is a proline-directed serine/threonine kinase enriched in post-mitotic neurons. CDK5 is activated when bound to p35 or p39 and phosphorylates many substrates, including regulators of cytoskeletal organization (Dhavan and Tsai, 2001). Several lines of evidence have indicated that CDK5 plays crucial roles in neuronal migration. In the cerebral cortex, radial migration of pyramidal cells shows severe defects in the absence of CDK5, including failures of transition from multipolar to bipolar morphologies and proper adhesion to radial glia (Gilmore et al., 1998; Gupta et al., 2003; Hatanaka et al., 2004; Ohshima et al., 2007). On the other hand, tangential migration of GABAergic interneurons in the cerebrum is less affected by CDK5 deficiency (Gilmore and Herrup, 2001). This raises the interesting possibility that CDK5 might be differentially involved in kinetics of radial and tangential migration. However,

it is yet unclear whether differential effects of CDK5 in pyramidal neurons and interneurons are due to its action in molecular kinetics specific for radial migration, or differential expression of CDK5 and/or related molecules in these cell types. Loss of CDK5 activity also affects migration of cerebellar granule cells (Chae et al., 1997; Ohshima et al., 1999; Hirasawa et al., 2004). To address the question of which aspects of biphasic migration of granule cells depend on CDK5, we established a time-lapse imaging system for quantitative analyses of biphasic migration of granule cells in cerebellar organotypic cultures. By combining this approach with in vivo analyses of granule cell migration in the cerebellar cortex, we found that radial migration was severely affected, while tangential migration was less affected in granule cells overexpressing a dominant-negative CDK5 mutant. The present data suggest the mode-specific regulation of cerebellar granule cell migration by CDK5.

Result

In vivo electroporation for specific gene transfer into pre-migratory granule cells

To elucidate migrating behaviors of cerebellar granule cells in vivo, we transfected pCAG-EGFP plasmids into postnatal day 8 (P8) mice cerebella by using an in vivo electroporation system (Umeshima et al., 2007). The plasmid DNA solution was injected into the primary fissure of the cerebellum (interlobular space between lobule V and VI), and electric pulses were then applied between the injecting syringe and the electrodes attached to the head. This enabled us to transduce plasmids specifically into immature granule cells and their progenitors in the outer EGL close to the injection site. Twenty-four hours after electroporation (P9), injected brains were fixed and sectioned. EGFP-labeled cells were seen only in the external granular layer (EGL), suggesting that plasmids were specifically incorporated in granule cell precursors in the EGL (Figure 1A, B). In the coronal sections, cells at the lower part of the EGL had long bipolar processes along the medio-lateral axis. These cells were considered as post-mitotic granule cells initiating tangential migration (data not shown, see Figure 3A). Forty-eight hours after electroporation (P10), $18.9 \pm 4.1\%$ (mean $\pm$ s.d.; n = 12 slices from 3 brains, >300 cells counted) of EGFP+ cells were seen in the molecular layer (ML). They elongated leading processes toward the internal granular layer (IGL) and underwent radial migration. The majority of EGFP+ cells ($52.2 \pm 13.4\%$) were located in the EGL,

6

while some cells (20.4 ± 12.2%) already reached the IGL. At P11 (72nd hour of electroporation), more EGFP+ cells were settled in the IGL (50.0 ± 6.9%) at the expense of those in the EGL (25.2 ± 9.2%). After P12 (96th hour and later), most EGFP + cells finished migration and were located in the IGL (83.0 ± 5.9% at 96 h and 92.8 ± 6.6% at 120 h, respectively) except for a small number of cells that were still resided in the EGL or ML. Mature granule cells were broadly distributed throughout the IGL with a slight increment in the upper half (54.8 ± 6.2% upper vs 38.1 ± 8.7% lower at 120 h). Thus the time course of granule cell migration could be quantitatively analyzed by the present in vivo electroporation approach. In the following experiments, we analyzed tangential and radial migration of transfected cells at 24 and 48 hours after electroporation, respectively, when each phase of migration was dominantly observed.

A dominant negative form of CDK5 cell-autonomously inhibits cerebellar granule cell migration in vivo

Previous studies using knock-out mice have indicated that loss of CDK5 activity causes defects in cerebellar granule cell migration in vivo (Chae et al., 1997; Ohshima et al., 1999; Hirasawa et al., 2004). Here we electroporated a dominant negative construct of CDK5 (CDK5-DN, a kinase-dead K33T mutant; Nikolic et al., 1996) together with EGFP to inhibit cell-intrinsic CDK5 activity in the granule cells in vivo. Six days after

electroporation, the majority of CDK5-DN-transfected cells (52.5 ± 1.7%, mean ± s.e.m., n = 24 slices from 3 brains, >1000 cells counted) failed to reach the IGL and ectopically located in the ML or PCL (Figure 2A, B). This was in contrast to control cells electroporated with only EGFP that had mostly reached the IGL and only a small portion remained in the ML or PCL (13.0 ± 1.2%, n = 24 slices from 3 brains, >1000 cells counted). In addition, many CDK5-DN-transfected cells stopped in the upper half of the IGL, while the percentage of cells that reached the lower IGL was reduced (35.0 ± 1.9% in the upper IGL vs 12.5 ± 0.9% in the lower IGL in CDK5-DN condition, compared to 54.7 ± 1.4% vs 32.4 ± 1.3% in control). These results support the notion that inhibition of CDK5 disrupts cerebellar granule cell migration in a cell-autonomous manner (Ohshima et al., 1999).

<u>CDK5 inhibition has minor effects on tangential migration</u>

Next, we asked whether CDK5 differentially contributed to tangential and radial migration of granule cells. We first investigated the effect of CDK5-DN on morphology of granule cells during tangential migration in vivo by using fixed tissue samples. During tangential migration, granule cells took a bipolar shape with leading and trailing processes along the medio-lateral axis of the cerebellum (Figure 3A). The length of the leading process differed among individual cells as it kept growing during tangential

migration (Figure 3C, D). CDK5-DN expression did not alter bipolar morphology of granule cells (Figure 3B). Leading processes of CDK5-DN-expressing granule cells also varied in length with no significant difference from those of control cells (Figure 3C, D).

To further investigate the effect of CDK5-DN on tangential migration, kinetics of tangential migration was examined by live-cell imaging in an organotypic culture. We previously developed a time-lapse imaging system to observe radial migration of EGFP-labeled cerebellar granule cells in coronal cerebellar slices (Umeshima et al., 2007). It was, however, difficult to demarcate individual granule cell shapes during tangential migration by the previous method, because of the high cell density in the EGL. We therefore modified the imaging approach for observation of tangential migration. One day after electroporation, cerebellar lobes containing many transfected cells were identified and isolated under a fluorescent microscope. The isolated lobe was put on a millipore filter and observed through the superficial layer of the EGL (Supplemental Figure S1). Using this approach, we successfully captured the kinetics of individual granule cells undergoing tangential migration along the longitudinal axis of the EGL (Figrue 3E; see also Supplemental Movie 1). The architecture of the cerebellar cortex was conserved in this condition (Supplemental Figure S2A) Granule cells exhibited a long bipolar shape and migrated in both medial

and lateral directions consistent with previous observation (Ryder and Cepko, 1994; Komuro et al., 2001). In some cases, the trailing process took over the leading process on the other side so that the cells moved in opposite directions during a recording period of 8 hours (9 cells out of 50 cells). Some trailing processes were retracted while others were retained throughout the recording period. In most cases the leading process moved faster than the soma so that the leading process gradually elongated during tangential migration, consistent with the observations in fixed tissues (Figure 3E', E'', G). Although CDK5-DN induced no obvious morphological change of tangentially migrating granule cells, there was a slight but significant reduction in migration speed (Figure 3F-F'', G; see also Supplemental Movie 2). Both the soma and leading process of CDK5-DN cells moved more slowly than those of control cells. These results suggest that CDK5 activity is involved in regulation of motility but is dispensable for the bipolar morphology of granule cells during tangential migration.

CDK5 inhibition causes severe morphological defects in radially migrating granule cells

Next, we examined the effect of CDK5-DN on radial migration of granule cells. CDK5 inhibition caused ectopic localization of granule cells in the ML (Figure 2). Many of these ectopic CDK5-DN-transfected cells bore leading processes pointing toward the

IGL, suggesting that CDK5-DN did not disturb the transition from tangential migration to radial migration. Consistently, the majority of CDK5-DN cells (87.4 ± 1.1%) had left the EGL and were located in the deeper layers at P12 (see Figure 2). Thus we focused on cell morphology of radially migrating granule cells. During radial migration in vivo, normal granule cells had shorter leading processes with less variance in length than tangentially migrating cells (Figure 4A, C, D, see also Figure 3A, C, D). CDK5-DN expression induced drastic changes in the morphology of radially migrating granule cells. We found two distinct types of morphological changes in CDK5-DN-expressing cells. The first type had an aberrantly elongated leading process (Figure 4B-D). The second type had multiple and/or branched leading processes (Figure 4B', E). Some cells exhibited mixed phenotypes and bore multiple long leading processes (see cells at the right side in Figure 4B).

Next, kinetics of radially migrating granule cells was observed by live-cell imaging using coronal cerebellar slices prepared at P10 (48 hour after electroporation). We confirmed that our slice preparation did not disrupt the architecture of the cerebellar cortex (Supplemental Figure S2B). In control, among 52 cells undergoing radial migration in the EGL or ML at the onset of observation, 32 cells (61.5%) reached the IGL during the recording period of 12 hours (Figure 5A; see also Supplemental Movie 3). Most cells migrated directly toward the IGL except for 2 cells which moved in the

opposite direction. The leading process tip and soma migrated at similar speeds so that

the leading process remained constant in length during radial migration in contrast to

that of tangential migration (Figure 5D, D'). This was consistent with the result

obtained by fixed tissue observation. In CDK5-DN-expressing cells, the migratory

speed was significantly reduced (Figure 5F) and only 17.0% of granule cells (9 cells out

of 53 cells) reached the IGL during 12 hours of recording. We also confirmed two types

of morphological defects seen in fixed tissue samples; some granule cells (13 cells)

failed to move the cell soma but aberrantly elongated their leading processes (Figure

5B, E, E', see also Supplemental Movie 4). Other 16 cells failed to keep single leading

processes and repeated retraction and elongation of unstable processes (Figure 5C, see

also Supplemental Movie 5). These two phenotypes were concurrently seen in the same

cells in 4 cases. These results indicate that CDK5 inhibition severely disrupts the

kinetics of radial migration of granule cells.

Interestingly, some radial processes of CDK5-DN-expressing cells overshot

the IGL and invaded into axonal tracts in the white matter at 5 day after electroporation

(Figure 4F). Some of these ectopic fibers were derived from heterotopic granule cells in

the ML (Figure 4G). Thus, unlike the leading process of normal granule cells that

differentiates into a dendrite after completion of migration, the elongated leading

process of CDK5-DN-expressing granule cells was likely to form an aberrant axon-like

fiber in the cerebellar cortex.

CDK5 inhibition does not affect association of the leading process to glial fibers

We next addressed how CDK5-DN affected the radial migration. Cerebellar granule cells are thought to move along radial fibers of Bergmann glia during radial migration. It has been suggested that CDK5 is involved in attachment of the leading process of migrating pyramidal neurons to radial glial fibers in the cerebral cortex (Gupta et al., 2003). These observations led us to examine if CDK5 inhibition affected attachment of the leading process to Bergmann glial fibers in vivo. In normal cells, EGFP-labeled radial leading processes were closely apposed to GFAP-positive glial fibers (Supplemental Movie 6). We found that CDK5-DN-expressing granule cells also attached their long leading processes to the glial fibers (Supplemental Movie 7). This result suggests that migratory defects of CDK5-DN-expressing granule cells are unlikely due to abnormal adhesion to glial fibers.

Centrosomal movement is disrupted in CDK5-DN-expressing granule cells

Time-lapse imaging revealed that CDK5 inhibition severely disrupted nuclear migration (nucleokinesis) of granule cells especially in radial migration. We have previously indicated that nuclear and centrosomal migration involve distinct cytoskeletal controls

and that inhibition of some molecules regulating nuclear migration causes increment in the nucleus-centrosome (N-C) distance (Umeshima et al., 2007). We investigated whether CDK5 inhibition affected the N-C distance of radially migrating granule cells. To this end, a cell volume marker mRFP and a centrosomal marker Centrin-2-EGFP were co-electroporated with or without CDK5-DN into P8 mouse cerebellum. Two days after electroporation, the brains were fixed, sectioned and stained with DAPI to visualize the nuclei of granule cells. The N-C distance was defined as the distance between the front end of the nucleus and centrosome (Figure 6A). In 34.4% of granule cells the centrosome followed the front end of the nucleus, consistent with our previous studies. CDK5-DN did not increase the N-C distance, compared to that in control cells (Figure 6B). To further investigate the effect of CDK5-DN on centrosome behavior, we carried out time-lapse imaging of the centrosome in a cerebellar slice culture using transgenic mice which ubiquitously expressed GFP-Centrin-2 (Higginbotham et al., 2006). Consistent with the fixed sample data, the centrosome was located close to the soma in most granule cells at the onset of time-lapse imaging. In control cells, the centrosome migrated forward along with nuclear migration during the recording period (Figure 6C and E; see also Supplemental Movie 8). The centrosome in CDK5-DN-expressing cells failed to undergo constant forward movement but fluctuated within the cell soma (Figure 6D, D' and E; see also Supplemental Movie 9, 10). The speed of

forward movement of the centrosome was significantly reduced by CDK5-DN

expression (Figure 6F). These results indicate that CDK5 inhibition prevents not only

the nucleokinesis but also the centrosomal migration during radial migration.

<u>Discussion</u>

Recent studies have shown that kinetics and molecular mechanisms of neuronal migration vary between cell types and migrating modes. Cerebellar granule cells provide a beneficial model to investigate mode-specific regulation of neuronal migration in the same cells. Migration of cerebellar granule cells has been studied by using various primary culture systems of dissociated cells or tissue explants (Edmondson and Hatten, 1987; Nakatsuji and Nagata, 1989; Nagata and Nakatsuji, 1994; Guan et al., 2007). In return for their advantages in accessibility to cells, it is unclear whether cultured cells on artificial substrates would reproduce the same migration behavior in the laminated cortex in vivo. In the present study, we developed a live imaging system for quantitative analyses of tangential migration of cerebellar granule cells within intact cell architecture. In conjunction with quantitative analyses of radial migration that we previously established, we investigated the relative influences of CDK5 inhibition on biphasic migration of granule cells in the cerebellar cortex. We demonstrated that inhibition of CDK5 caused severe impairments in radial migration, while it caused only moderate decrease in the motility during tangential migration. Our organotypic culture systems conserved the cell architecture in the cerebellar cortex at least during the imaging period. Moreover, the cell morphologies observed in live-cell imaging were well correlated with those in fixed tissue samples. We thus think that dynamics and

mechanics of granule cell migration are recapitulated in the present organotypic culture systems.

We have previously reported that the leading processes utilized for tangential and radial migration have distinct molecular properties (Kawaji et al., 2004). The leading process for tangential migration expresses axonal proteins and gradually elongates to form a parallel fiber axon after completion of migration. On the other hand, the leading process for radial migration contains proteins enriched in dendrites and later differentiates into a dendritic process. In the present study, extension of the leading process for radial migration was tightly coupled with somal movement so that it kept constant length, while the leading process for tangential migration elongated independently of somal movement. Loss of CDK5 activity disrupted the coupling of the leading process and soma during radial migration, resulting in abnormal elongation or excess formation of multiple and/or branched leading processes. The aberrantly elongated leading processes appeared not to differentiate into dendrites but to form long thin processes along axonal tracts in the white matter. Although it was difficult to identify expression of axonal proteins in these processes within dense axon fascicles in the white matter, their morphology resembled axons. The aberrant elongation of the leading process was never seen in the cells defective in radial migration caused by inhibition of the LINC complex (linker of nucleoskeleton and cytoskeleton)

(unpublished data, Zhang et al., 2009). CDK5 may thus play important roles in the formation and maintenance of the leading process with dendritic characteristics. Consistent with this notion, CDK5-deficient pyramidal neurons exhibit severe morphological impairments in apical dendrites, while their axons are mostly intact in morphology with a slight misrouting defect (Ohshima et al., 2007).

We also asked if CDK5 regulated neuronal migration guided by specific substrates. Cerebellar granule cells migrate along glial fibers during radial migration, while they migrate along the preformed parallel fiber axons of other granule cells during tangential migration. CDK5 inhibition impairs glia-guided locomotion, but has little or no impact on glia-independent somal translocation in cerebral pyramidal neurons (Hatanaka et al., 2004). It has also been shown that adhesion of leading processes to glial fibers is disrupted by deletion of a CDK5 activator p35 in cerebral pyramidal neurons (Gupta et al., 2003). In contrast, we found no obvious defect in association of the leading process to glial fibers, questioning the role of CDK5 in neuron-glia interaction during granule cell migration. Recent studies have indicated that CDK5 deletion impairs chain migration of neuroblasts along neurites of other neuroblasts in the postnatal subventricular zone (SVZ; Hirota et al., 2007). In addition, it has been demonstrated that glia-independent tangential migration of cerebral inhibitory neurons is moderately affected by p35-deletion (Rakić et al., 2009). Attachment to glial fibers is

thus unlikely the principal mechanism regulated by CDK5.

Neuronal migration disorders are often accompanied by increase of the N-C distance (Tanaka et al., 2004a). The N-C distance in CDK5-DN-expressing granule cells was indistinguishable from that in normal cells. Live-cell imaging revealed that CDK5 inhibition severely disrupted forward migration of the centrosome and randomized their movement. We have previously shown that the nucleus migrates independently of the centrosome position and sometimes passes the centrosome (Umeshima et al., 2007). It has also been reported that nuclear and centrosome migration is regulated by at least partially distinct mechanisms (Tsai et al., 2007). Although the precise mechanisms remain elusive, CDK5 is involved in the regulation of both nuclear and centrosome migration.

A number of signaling molecules regulating centrosome migration have been identified. Among them, Sema6a-Plexin-A2 signaling is a feasible candidate for an upstream regulator of CDK5 that induces phosphorylation of CDK5 (Renaud et al., 2008). Mammalian homologues of Par proteins in *C. elegans*, Par6a, MARK2 and LKB1 have also been shown to regulate centrosome positioning and migration (Solecki et al., 2004; Sapir et al., 2008; Solecki et al., 2009; Asada and Sanada, 2010). Another mammalian Par protein, Pard3A triggers radial migration of cerebellar granule cells (Famulski et al., 2010).

CDK5 recognizes and phosphorylates many substrates related to neuronal migration. Phosphorylation of Ndel1, FAK and DCX by CDK5 is thought to affect nuclear migration through regulation of perinuclear microtubule structure (Niethammer et al., 2000; Sasaki et al., 2000; Xie et al., 2003; Shu et al., 2004; Tanaka et al., 2004b). On the other hand, CDK5 phosphorylates and stabilizes p27kip1, which regulates actin dynamics via RhoA-cofilin pathway in migrating neurons in the cerebral cortex (Kawauchi et al., 2006). Neurabin-I is another actin regulator phosphorylated by CDK5 (Causeret et al., 2007). CDK5 would coordinate microtubule and actin dynamics during neuronal migration through the phosphorylation of multiple substrates that are differentially involved in radial and tangential migration of granule cells. Further studies will elucidate the signaling pathway upstream and downstream of CDK5 during neuronal migration.

Materials and methods

cDNA constructs and mice

pCAG-EGFP, pCAG-Venus, pCAG-DsRed-express and pCentrin-2-EGFP were described previously (Umeshima et al., 2007; Sasaki et al., 2010). For construction of pCAG-CDK5-DN, the full-length CDK5 cDNA was cloned from a P7 ICR mouse whole brain cDNA library by PCR using the following primers.

CDK5 forward: CTCGAGGCCGCCATGCAGAAATACGAGAAACT

CDK5 reverse: GTCGACCTATGGGGGACAGAACTCA

Substitution of lysine 33 (AAG) for threonine (ACG) was performed by site-directed mutagenesis using the GeneEditor Kit (Promega) according to the manufacturer's instruction (Nikolic et al., 1996). The PCR product was fused with a HA-tag at the N-terminus and subcloned into pCAGGS.

GFP-Centrin-2 transgenic mice were purchased from Jackson Labs. Mice were handled in accordance with the Animal Experiment Committee of the RIKEN Brain Science Institute and Kyoto University and were housed in a dedicated pathogen-free environment with a 12 h light/dark cycle.

In vivo electroporation

In vivo electroporation into postnatal mouse cerebella was performed as previously described (Umeshima et al., 2007). Briefly, P8 ICR mice were anesthetized on ice and injected with plasmid DNAs (2.1 µg of each) diluted in 0.7 µl TE buffer in the interlobular space between lobule V and VI using a microsyringe with a 33-gauge needle connected to the anode. After injection, tweezer-type electrodes connected to the cathode were placed on the occipital regions, and electric pulses (6 pulses of 70 mV for 50 ms-duration with 150 ms-intervals) were applied using a pulse generator, CUY21 (Nepagene). The pups were revived at 37ºC and returned to the litter.

Time-lapse imaging

For time-lapse imaging of tangential migration, mouse brains were quickly dissected 1 day after electroporation, and transferred into ice-cold ACSF bubbled with a gas mixture of 95% O_2 and 5% CO_2. The lobes expressing transfected genes were identified and isolated under a fluorescent microscope and stripped meninges by forceps. For time-lapse imaging of radial migration, cerebella were dissected and embedded in 3% agarose 2 days after electroporation, and sectioned into 300 µm-thick coronal slices using a vibratome (linearslicer PRO 7, Dosaka EM).

Lobes or slices were placed on a Millicell-CM (Millipore), mounted in collagen gel and soaked in culture medium (15% heat-inactivated horse serum, 25%

Earle's balanced salt, 60% Eagle's basal medium, 5.6 g/l glucose, 3mM L-glutamine, 1.8 mg/ml NaHCO$_3$, 1mM sodium pyruvate, 5 µg/ml bovine insulin, 5 µg/ml human transferrin, 30 nM sodium selenite, 20 nM progesterone). The tissues in Millicell-CM dishes were kept at 37ºC in an incubator chamber attached to an upright microscope stage (BX61WI) and provided with constant gas flow (85% O$_2$, 5% CO$_2$, 10% air). After the tissues were allowed to settle for 2-4 hours, time-lapse images were obtained with a laser scanning confocal microscope (FV1000, Olympus).

For time-lapse imaging except for centrosome imaging, Venus YFP was utilized in place of EGFP. Centrosome kinetics were viewed through a 60x water-immersion objective (numerical aperture 1.10, Olympus). All other images were viewed through a 20x water-immersion objective (numerical aperture 0.50, Olympus). Ten to twenty optical Z sections at 10 µm (20x objective) or 2 µm (60x objective) steps were obtained and stacked to acquire whole images.

Immunofluorescence and image acquisition

To obtain images of tangentially migrating granule cells in fixed tissue samples, cerebellar lobes were isolated and fixed by 4% PFA. For radially migrating cells, brains were fixed in 4% PFA and sectioned into 50 µm-thick sagittal slices with a vibratome. For immunostaining of lobe/slice cultures, samples were fixed after recording in the

stage-top incubator. Lobe cultures were cryoprotected in 20% sucrose/PBS, and then sectioned into 20 µm-thick transverse slices with a cryostat (CM1900, Leica). Immunofluorescence of cerebeller sections was performed as previously described. The following antibodies were used; anti-GFAP (1:1000, rabbit polyclonal, Chemicon); anti-Calbindin D-28K (1:1000, mouse monoclonal, Swant). For secondary detection, Alexa568- or 633-conjugated anti-rabbit or mouse IgG (1:400, Invitrogen) were used. Image acquisition was carried out with a laser-confocal microscope Fluoview FV1000 (Olympus) using a 40x objective (numerical aperture 0.95, Olympus) and a 100x oil-immersion objective (numerical aperture 1.4, Olympus). Optical Z sections were obtained and stacked to acquire whole images.

<u>Statistical Analysis</u>

Statistical analyses were performed with Excel (Microsoft) and R (http://www.r-project.org). Normality was assessed by the Shapiro-Wilk test, and where data were not normally distributed, statistical differences between data sets were tested by Wilcoxon rank sum. As for normally distributed data, the equality of variance between data sets was assessed by F-tests. Data sets with equal variance were compared by two-tailed unpaired Student t-tests whereas data sets with non-equal variance were compared by two-tailed unpaired t-tests with Welch's correction.

Acknowledgement

References

Asada, N., Sanada, K., 2010. LKB1-mediated spatial control of GSK3beta and adenomatous polyposis coli contributes to centrosomal forward movement and neuronal migration in the developing neocortex. J Neurosci 30, 8852–8865.

Causeret, F., Jacobs, T., Terao, M., Heath, O., Hoshino, M., Nikolić, M., 2007. Neurabin-I is phosphorylated by Cdk5: implications for neuronal morphogenesis and cortical migration. Mol Biol Cell 18, 4327–4342.

Chae, T., Kwon, Y.T., Bronson, R., Dikkes, P., Li, E., Tsai, L.-H., 1997. Mice Lacking p35, a Neuronal Specific Activator of Cdk5, Display Cortical Lamination Defects, Seizures, and Adult Lethality. Neuron 18, 29–42.

Dhavan, R., Tsai, L.-H., 2001. A DECADE OF CDK5. Nat Rev Mol Cell Biol 2, 749–759.

Edmondson, J.C., Hatten, M.E., 1987. Glial-guided granule neuron migration in vitro: a high-resolution time-lapse video microscopic study. J Neurosci 7, 1928–1934.

Famulski, J.K., Trivedi, N., Howell, D., Yang, Y., Tong, Y., Gilbertson, R., Solecki, D.J., 2010. Siah regulation of Pard3A controls neuronal cell adhesion during germinal zone exit. Science 330, 1834–1838.

Gilmore, E.C., Ohshima, T., Goffinet, A.M., Kulkarni, A.B., Herrup, K., 1998. Cyclin-

dependent kinase 5-deficient mice demonstrate novel developmental arrest in cerebral cortex. J Neurosci 18, 6370–6377.

Gilmore, E.C., Herrup, K., 2001. Neocortical cell migration: GABAergic neurons and cells in layers I and VI move in a cyclin-dependent kinase 5-independent manner. J Neurosci 21, 9690–9700.

Guan, C.-B., Xu, H.-T., Jin, M., Yuan, X.-B., Poo, M.-M., 2007. Long-range Ca2+ signaling from growth cone to soma mediates reversal of neuronal migration induced by slit-2. Cell 129, 385–395.

Gupta, A., Sanada, K., Miyamoto, D.T., Rovelstad, S., Nadarajah, B., Pearlman, A.L., Brunstrom, J., Tsai, L.-H., 2003. Layering defect in p35 deficiency is linked to improper neuronal-glial interaction in radial migration. Nat Neurosci 6, 1284–1291.

Hatanaka, Y., Hisanaga, S.-I., Heizmann, C.W., Murakami, F., 2004. Distinct migratory behavior of early- and late-born neurons derived from the cortical ventricular zone. J Comp Neurol 479, 1–14.

Higginbotham, H., Tanaka, T., Brinkman, B.C., Gleeson, J.G., 2006. GSK3beta and PKCzeta function in centrosome localization and process stabilization during Slit-mediated neuronal repolarization. Mol Cell Neurosci 32, 118–132.

Hirasawa, M., Ohshima, T., Takahashi, S., Longenecker, G., Honjo, Y., Veeranna, Pant,

H.C., Mikoshiba, K., Brady, R.O., Kulkarni, A.B., 2004. Perinatal abrogation of Cdk5 expression in brain results in neuronal migration defects. Proc Natl Acad Sci USA 101, 6249–6254.

Hirota, Y., Ohshima, T., Kaneko, N., Ikeda, M., Iwasato, T., Kulkarni, A.B., Mikoshiba, K., Okano, H., Sawamoto, K., 2007. Cyclin-dependent kinase 5 is required for control of neuroblast migration in the postnatal subventricular zone. J Neurosci 27, 12829–12838.

Kawaji, K., Umeshima, H., Eiraku, M., Hirano, T., Kengaku, M., 2004. Dual phases of migration of cerebellar granule cells guided by axonal and dendritic leading processes. Mol Cell Neurosci 25, 228–240.

Kawauchi, T., Chihama, K., Nabeshima, Y.-I., Hoshino, M., 2006. Cdk5 phosphorylates and stabilizes p27kip1 contributing to actin organization and cortical neuronal migration. Nat Cell Biol 8, 17–26.

Komuro, H., Rakic, P., 1998. Distinct modes of neuronal migration in different domains of developing cerebellar cortex. J Neurosci 18, 1478–1490.

Komuro, H., Yacubova, E., Yacubova, E., Rakic, P., 2001. Mode and tempo of tangential cell migration in the cerebellar external granular layer. J Neurosci 21, 527–540.

Nagata, I., Nakatsuji, N., 1994. Migration behavior of granule cell neurons in cerebellar

cultures I. A PKH26 labeling study in microexplant and organotypic cultures. Development, Growth & Differentiation 36, 19–27.

Nakatsuji, N., Nagata, I., 1989. Paradoxical perpendicular contact guidance displayed by mouse cerebellar granule cell neurons in vitro. Development 106, 441–447.

Niethammer, M., Smith, D.S., Ayala, R., Peng, J., Ko, J., Lee, M.S., Morabito, M., Tsai, L.H., 2000. NUDEL is a novel Cdk5 substrate that associates with LIS1 and cytoplasmic dynein. Neuron 28, 697–711.

Nikolic, M., Dudek, H., Kwon, Y.T., Ramos, Y.F., Tsai, L.H., 1996. The cdk5/p35 kinase is essential for neurite outgrowth during neuronal differentiation. Genes Dev 10, 816–825.

Ohshima, T., Gilmore, E.C., Longenecker, G., Jacobowitz, D.M., Brady, R.O., Herrup, K., Kulkarni, A.B., 1999. Migration defects of cdk5(-/-) neurons in the developing cerebellum is cell autonomous. J Neurosci 19, 6017–6026.

Ohshima, T., Hirasawa, M., Tabata, H., Mutoh, T., Adachi, T., Suzuki, H., Saruta, K., Iwasato, T., Itohara, S., Hashimoto, M., Nakajima, K., Ogawa, M., Kulkarni, A.B., Mikoshiba, K., 2007. Cdk5 is required for multipolar-to-bipolar transition during radial neuronal migration and proper dendrite development of pyramidal neurons in the cerebral cortex. Development 134, 2273–2282.

Rakic, P., 1990. Principles of neural cell migration. Experientia 46, 882–891.

Rakić, S., Yanagawa, Y., Obata, K., Faux, C., Parnavelas, J.G., Nikolić, M., 2009. Cortical interneurons require p35/Cdk5 for their migration and laminar organization. Cerebral Cortex 19, 1857–1869.

Renaud, J., Kerjan, G., Sumita, I., Zagar, Y., Georget, V., Kim, D., Fouquet, C., Suda, K., Sanbo, M., Suto, F., Ackerman, S.L., Mitchell, K.J., Fujisawa, H., Chédotal, A., 2008. Plexin-A2 and its ligand, Sema6A, control nucleus-centrosome coupling in migrating granule cells. Nat Neurosci 11, 440–449.

Ryder, E.F., Cepko, C.L., 1994. Migration patterns of clonally related granule cells and their progenitors in the developing chick cerebellum. Neuron 12, 1011–1029.

Sapir, T., Sapoznik, S., Levy, T., Finkelshtein, D., Shmueli, A., Timm, T., Mandelkow, E.-M., Reiner, O., 2008. Accurate balance of the polarity kinase MARK2/Par-1 is required for proper cortical neuronal migration. J Neurosci 28, 5710–5720.

Sasaki, N., Kurisu, J., Kengaku, M., 2010. Sonic hedgehog signaling regulates actin cytoskeleton via Tiam1-Rac1 cascade during spine formation. Mol Cell Neurosci 45, 335–344.

Sasaki, S., Shionoya, A., Ishida, M., Gambello, M.J., Yingling, J., Wynshaw-Boris, A., Hirotsune, S., 2000. A LIS1/NUDEL/cytoplasmic dynein heavy chain complex in the developing and adult nervous system. Neuron 28, 681–696.

Shu, T., Ayala, R., Nguyen, M.-D., Xie, Z., Gleeson, J.G., Tsai, L.-H., 2004. Ndel1

operates in a common pathway with LIS1 and cytoplasmic dynein to regulate cortical neuronal positioning. Neuron 44, 263–277.

Solecki, D.J., Model, L., Gaetz, J., Kapoor, T.M., Hatten, M.E., 2004. Par6alpha signaling controls glial-guided neuronal migration. Nat Neurosci 7, 1195–1203.

Solecki, D.J., Trivedi, N., Govek, E.-E., Kerekes, R.A., Gleason, S.S., Hatten, M.E., 2009. Myosin II motors and F-actin dynamics drive the coordinated movement of the centrosome and soma during CNS glial-guided neuronal migration. Neuron 63, 63–80.

Tanaka, T., Serneo, F.F., Higgins, C., Gambello, M.J., Wynshaw-Boris, A., Gleeson, J.G., 2004a. Lis1 and doublecortin function with dynein to mediate coupling of the nucleus to the centrosome in neuronal migration. J Cell Biol 165, 709–721.

Tanaka, T., Serneo, F.F., Tseng, H.C., Kulkarni, A.B., Tsai, L.-H., Gleeson, J.G., 2004b. Cdk5 phosphorylation of doublecortin ser297 regulates its effect on neuronal migration. Neuron 41, 215–227.

Tsai, J.-W., Bremner, K.H., Vallee, R.B., 2007. Dual subcellular roles for LIS1 and dynein in radial neuronal migration in live brain tissue. Nat Neurosci 10, 970–979.

Umeshima, H., Hirano, T., Kengaku, M., 2007. Microtubule-based nuclear movement occurs independently of centrosome positioning in migrating neurons. Proc Natl

Acad Sci USA 104, 16182–16187.

Xie, Z., Sanada, K., Samuels, B.A., Shih, H., Tsai, L.-H., 2003. Serine 732 phosphorylation of FAK by Cdk5 is important for microtubule organization, nuclear movement, and neuronal migration. Cell 114, 469–482.

Zhang, X., Lei, K., Yuan, X., Wu, X., Zhuang, Y., Xu, T., Xu, R., Han, M., 2009. SUN1/2 and Syne/Nesprin-1/2 complexes connect centrosome to the nucleus during neurogenesis and neuronal migration in mice. Neuron 64, 173–187.

Figure captions

Fig. 1. Time course of migration of EGFP-labeled cerebellar granule cells in vivo

Granule cells in the EGL were electroporated with a pCAG-EGFP plasmid on P8. Brains were fixed at 24, 48, 72, 96 and 120 hours after electroporation and sectioned into 50 µm-thick sagittal slices. (A) EGFP-labeled granule cells (green), all of which were located in the EGL at P9 (24 h), started radial migration at P10 (48 h) and almost finished immigration into the IGL at P12 (96 h). Each layer was identified by counterstaining with DAPI (blue in right panels). Scale bar represents 50 µm. EGL; the external granular layer, ML; the molecular layer, PCL; the Purkinje cell layer, IGL; the internal granular layer. (B) The percentages of total EGFP-labeled granule cells located in each layer at indicated time points. Data were obtained from 12 slices of 3 brains (>300 cells) in each stage. The IGL was subdivided into upper (IGL1) and lower (IGL2) halves. Error bars represent standard deviations.

Fig. 2. Inhibition of CDK5 disrupts granule cell migration in a cell-autonomous manner

Granule cells in the P8 mouse EGL were electroporated with either pCAG-EGFP alone (control), or pCAG-EGFP and pCAG-CDK5-DN. Sagittal sections were made 6d after electroporation. (A) In contrast to control granule cells that were mostly located within

33

the IGL, the cells overexpressing CDK5-DN failed to reach the IGL but accumulated in the ML and PCL . Each layer was identified by counterstaining with DAPI (blue in right panels). Scale bars indicate 50 µm. (B) The percentages of granule cells transduced with/without CDK5-DN located in each layer. The ML and IGL were divided into upper and lower halves. Data were obtained from 24 slices of 3 brains (>1000 cells) for each condition. Error bars indicate s.e.m. *p < 0.001, Student's t-test.

Fig. 3. Inhibition of CDK5 does not affect morphology and kinetics of granule cells during tangential migration

Granule cells were electroporated with either pCAG-EGFP alone (control) or pCAG-EGFP and pCAG-CDK5-DN at P8 and the transfected lobes were isolated and fixed after 24 hours. (A), (B) Granule cells undergoing tangential migration were observed through the superficial layer of granule cell precursors. Both control cells (A) and cells overexpressing CDK5-DN (B) showed bipolar morphology with leading processes of variable length. Scale bars indicate 10 µm. (C), (D) Distribution of the length of leading processes. (C) The length of leading processes is represented along the x axis and the percentages of total cell number in each bin are represented along the y axis. (D) Data in boxplots are represented as 25%-75% quartiles (boxes) and median (lines). Lower and higher whiskers indicate the lowest and highest data within 1.5 interquartile range (IQR)

of the respective quartiles. Outliers are represented by circles. There was no significant difference in the length (Wilcoxon rank sum test, p = 0.6423, n = 195 cells, control, n = 263 cells, CDK5-DN). (E)-(F") Time-lapse imaging of tangential migration of control cells transfected with Venus YFP alone (E-E"; see also Supplemental Movie 1), and cells overexpressing CDK5-DN (F-F"; see also Supplemental Movie 2). Leading processes gradually elongated during tangential migration in both control and CDK5-DN cells. CDK5-DN did not halt somal movement. Images were taken 20 min interval for 8 hours. Arrows and arrowheads indicate leading process tips and cell soma, respectively. Tracings of the cells indicated by arrows and arrowheads are shown in right panels of (E) and (F). Times are indicated in min. Scale bars represent 20 μm. Displacement of leading process tips and cell soma (E' and F'), and length of leading processes (E" and F") of the granule cells shown in (E) and (F) are plotted against time, respectively. (G) The average speed of cell soma and leading process tips (cell soma: n = 50 cells, control, n = 63 cells, CDK5-DN; leading process tips: n = 31 cells, control, n = 35 cells, CDK5-DN). *p < 0.05, **p < 0.001; Welch's t-test.

Fig. 4. Inhibition of CDK5 disrupts morphology of granule cells during radial migration

Granule cells were electroporated with either pCAG-EGFP alone (control), or pCAG-

EGFP and pCAG-CDK5-DN at P8 and analyzed in sagittal sections at 48 hours of electroporation. (A) Control granule cells undergoing radial migration had leading processes with constant length. (B), (B') CDK5-DN expression disrupted granule cell morphology and caused aberrantly longer leading processes (B) or multiple and/or branched leading processes (B'). Scale bars indicate 10 µm. (C) The length of leading processes is represented along the x axis and the percentages of total cell number in each bin are represented along the y axis. The longest leading process was counted for the cells with multiple leading processes. (D) Data in boxplots are represented as 25%-75% quartiles (boxes) and median (lines). Lower and higher whiskers indicate the lowest and highest data within 1.5 IQR of the respective quartiles. Outliers are represented by circles. Leading processes of cells expressing CDK5-DN were significantly longer than those of control cells. (n = 467 cells, control, n = 375 cells, CDK5-DN). *p < 0.001; Wilcoxon rank sum test. (E) The percentages of radially migrating granule cells with the indicated number of leading processes. (F and G) Granule cells expressing CDK5-DN elongated long and thin processes into the white matter (WM) after 5 days of electroporation. Dotted lines in (F) indicate borders between the WM and IGL. Each layer was identified by counterstaining with DAPI. Arrowheads in (G) trace a long radial process elongated into the WM from a granule cell in the ML. Scale bars indicate 50 µm in (F) and 20 µm in (G).

Fig. 5. Time-lapse imaging reveals that inhibition of CDK5 disrupts kinetics of radial migration of granule cells

Time-lapse imaging of radially migrating granule cells, expressing either Venus YFP alone (control; A, D and D', see also Supplemental Movie 3) or Venus YFP with CDK5-DN (B, C, E and E'; see also Supplemental Movie 4, 5). (A) Leading process tips and soma of control cells migrated at the same speed so that the leading processes remained constant in length. (B), (C) CDK5-DN expression halted somal movement and caused abnormal elongation of leading processes (B) or repeated extension and retraction of multiple leading processes (C). Panels are oriented the pial side up, with the white matter side down. Arrows and arrowheads indicate leading process tips and cell soma, respectively. Numbers attached to arrows represent the same processes among the sequential images. Tracings of the cells indicated by arrows and arrowheads are shown in lower panels of (A), (B) and (C). Images were taken 20 min interval for 12 hours. Times are indicated in min. Scale bars indicate 20 μm. (D-E') Displacement of leading process tips and cell soma (D and E), and length of leading processes (D' and E') of the granule cells shown in (A) and (B) are plotted against time, respectively. (F) The average speed of somal movement (n = 52 cells, control, n = 53 cells, CDK5-DN). Displacement toward the pial surface was defined as a negative value. Data in boxplots

are represented as 25%-75% quartiles (boxes) and median (lines). Lower and higher

whiskers indicate the lowest and highest data within 1.5 IQR of the respective quartiles.

Outliers are represented by circles. *p < 0.001, Wilcoxon rank sum test.

Fig. 6. Inhibition of CDK5 impairs centrosome migration during radial migration

(A), (B) Statistical analyses of the centrosome position in granule cells electroporated

with pCAG-DsRed-express and pCentrin-2-EGFP (control) or pCAG-DsRed-express,

pCentrin-2-EGFP and pCAG-CDK5-DN(CDK5-DN) at 48 hour after electroporation.

The nuclei were visualized by DAPI staining and the distance between the centrosome

and leading pole of the nucleus (N-C distance) was measured. (A) The distance from the

leading pole of the nucleus (point 0) to the leading process (plus; right) and the soma

(minus; left) are represented along the x axis and the percentages of total cell number in

each bin are represented along the y axis. (B) Data in boxplots are represented as

25%-75% quartiles (boxes) and median (lines). Lower and higher whiskers indicate the

lowest and highest data within 1.5 IQR of the respective quartiles. Outliers are

represented by circles. There is no significant difference in the N-C distance between

control cells and cells expressing CDK5-DN (0.7 ± 3.7 µm, n = 93 cells, control, 0.6 ±

2.5 µm, n = 90 cells, CDK5-DN, mean ± s.d., p = 0.7313, Wilcoxon rank sum test). (C)-

(D') Time-lapse images of centrosome movement during radial migration. Granule cells

in GFP-Centrin-2 mice were electroporated with pCAG-DsRed-express alone (C; see also Supplemental Movie 8) or pCAG-DsRed-express with pCAG-CDK5-DN (D and D'; see also Supplemental Movie 9, 10). Images were taken 5 min interval for 2-3 hours. Sequential images of 10 min are shown. Centrosomes labeled with GFP-Centrin-2 (green) are indicated by asterisks. Panels are oriented the pial side up, with the white matter side down. Scale bars indicate 5 µm. The centrosome was located close to the soma in most granule cells at the onset of time-lapse imaging (the distance between the centrosome and centroid of the soma: 8.5 ± 4.2 µm, control, n = 15 cells vs 3.5 ± 1.4 µm, CDK5-DN, n = 16 cells, mean $\pm$ s.d.). (E) Representative traces of displacement of the centrosome in cells expressing either pDsRed-express alone (control), or pDsRed-express with CDK5-DN (CDK5-DN) during a recording period of 3 hours. Red circles and red squires indicate the position at the onset and end of recording, respectively. In contrast to the centrosome in control cells which constantly migrated forward, the centrosome of CDK5-DN cells fluctuated within the soma and failed to undergo constant forward movement. (F) The average speed of forward movement of the centrosome. Data in boxplots are represented as 25%-75% quartiles (boxes) and median (lines). Lower and higher whiskers indicate the lowest and highest data within 1.5 IQR of the respective quartiles. Individual data are plotted by circles. CDK5-DN expression significantly reduced the forward movement of the centrosome

(5.9 ± 1.5 µm/h, n = 15 cells, control; 2.3 ± 0.6 µm/h, n = 16 cells, CDK5-DN, mean ±

s.e.m.,*p < 0.01, Wilcoxon rank sum test).

Figure S1. A schematic illustration of tangential migration in isolated cerebellar lobes

Cerebellar lobes transduced with fluorescent genes were isolated and maintained in an incubator chamber attached to an upright microscope stage. Images were acquired through the superficial layer of the cerebellar cortex. Many granule cells elongating their processes along the longitudinal axis were clearly visualized.

Figure S2. Lobe/slice cultures maintain the architecture of the cerebellar cortex

(A, B) Lobe cultures (A) and slice cultures (B) transfected with EGFP (green) were fixed after 6-hour incubation in a stage-top incubator. Lobe cultures were cryosectioned into 20 µm-thick transverse slices. Samples were immunostained with antibodies against GFAP (glial fibers; magenta) and Calbindin (Purkinje cells; yellow), and then counterstained by DAPI (blue). Each layer of the cerebellar cortex (the EGL, ML, PCL and IGL) was clearly distinguishable in both lobe and slice cultures. Bergmann glial fibers and Purkinje cell dendrites appeared to be intact in the ML. Tangential migration of EGFP-labelled granule cells was seen in the lower part of the EGL (A, B), and radially migrating cells were detected in the ML (B). Scale bars indicate 50 µm.

Movie 1

Tangential migration of the control granule cells depicted in Figure 3E. Images were acquired at 20-min-intervals for 8 hours; playback rate is 8 frames per s.
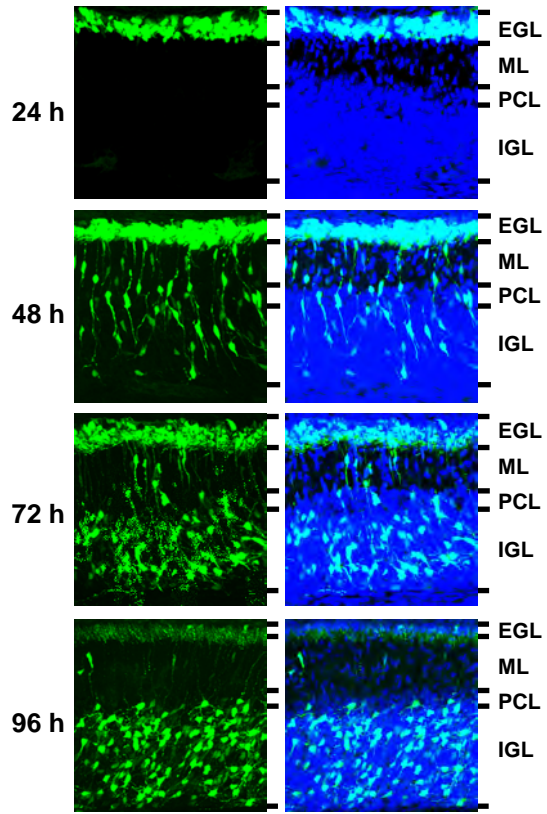
Movie 2

Tangential migration of the granule cells expressing CDK5-DN depicted in Figure 3F. Images were acquired at 20-min-intervals for 8 hours; playback rate is 8 frames per s.

Movie 3

Radial migration of the control granule cells depicted in Figure 5A. Images were acquired at 20-min-intervals for 12 hours; playback rate is 8 frames per s.

Movie 4

Radial migration of the granule cells expressing CDK5-DN depicted in Figure 5B. Images were acquired at 20-min-intervals for 12 hours; playback rate is 8 frames per s.

Movie 5

Radial migration of the granule cells expressing CDK5-DN depicted in Figure 5C.

Movie 6

Sagittal sections of cerebelli electroporated with pCAG-EGFP (green) were immunostained with anti-GFAP antibody (magenta). Optical Z sections were obtained and 3D-reconstructed images were rotated every 30 degrees.

Movie 7

3D-reconstructed images of the granule cell expressing CDK5-DN. Images were rotated every 30 degrees.

Movie 8

Centrosome kinetics in the control granule cells depicted in Figure 6C. Images were acquired at 5-min intervals for 3 hours; playback rate is 8 frames per s.

Movie 9

Centrosome kinetics in the granule cells expressing CDK5-DN depicted in Figure 6D. Images were acquired at 5-min intervals for 3 hours; playback rate is 8 frames per s.

Movie 10

Centrosome kinetics in the granule cells expressing CDK5-DN depicted in Figure 6D'.

Figure 1

Figure 2

A

B
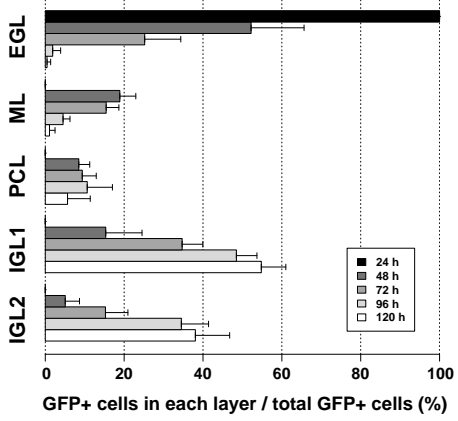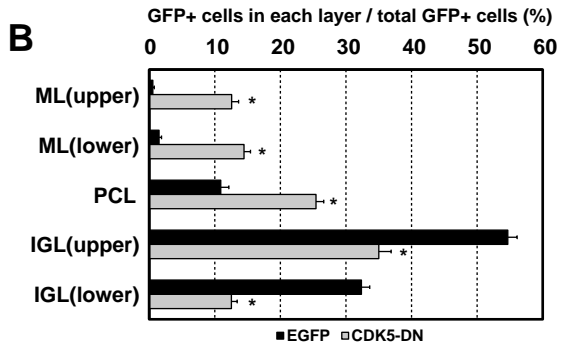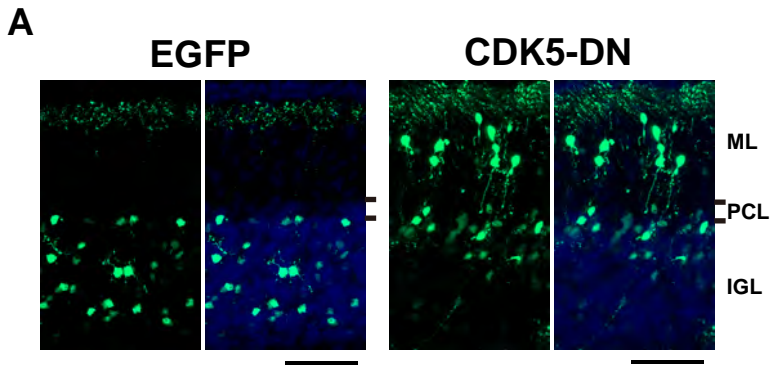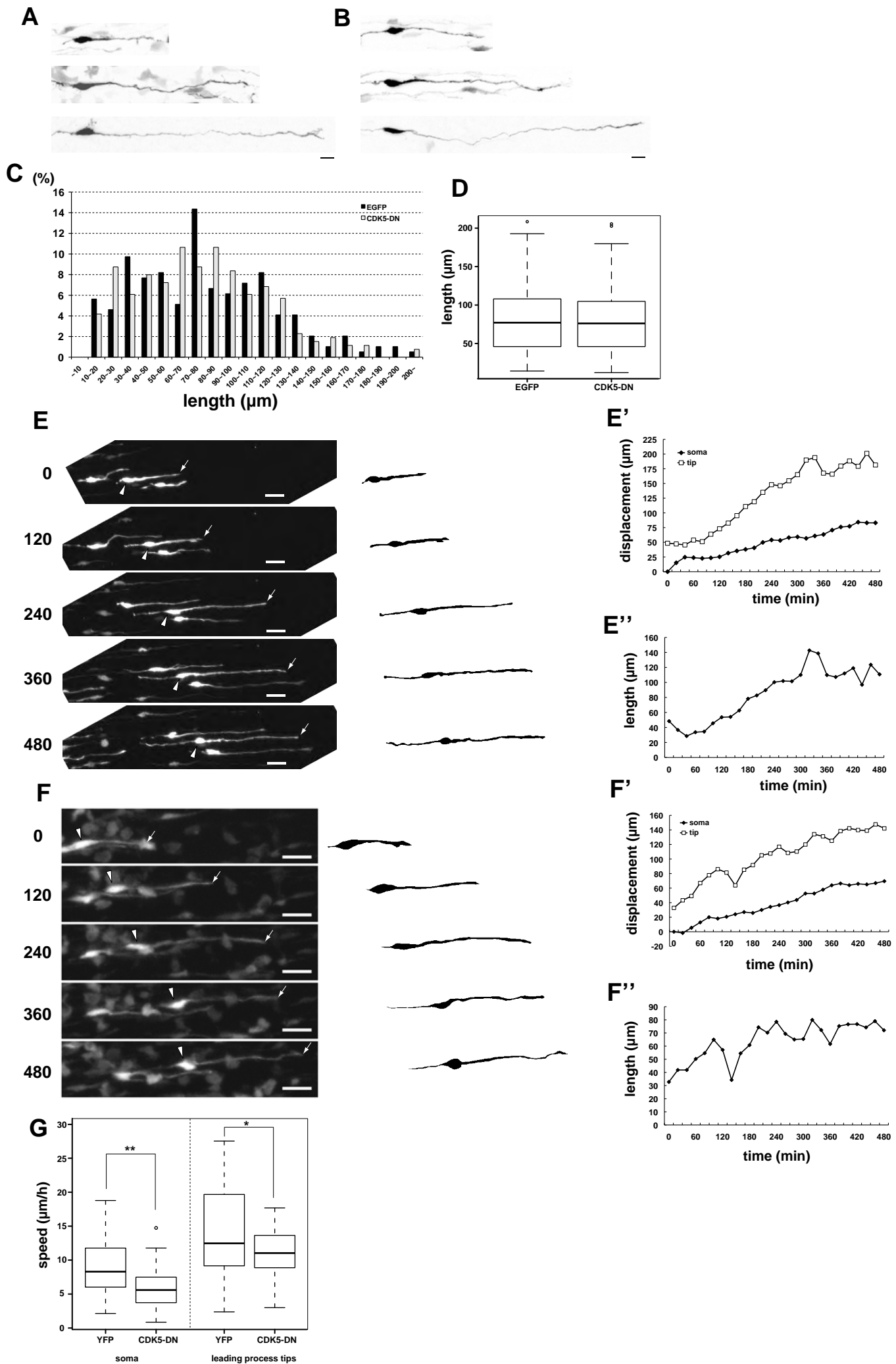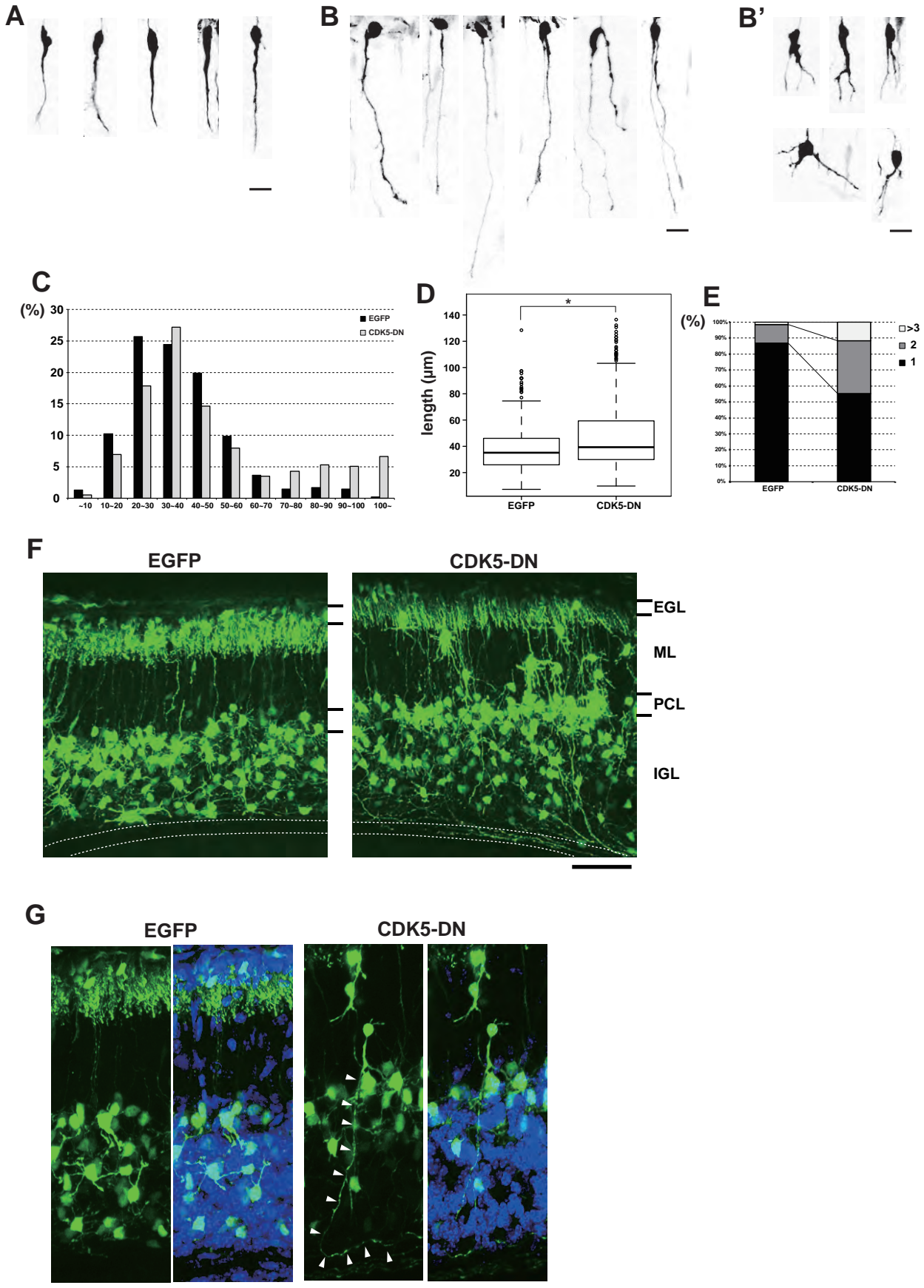
Figure 3

Figure 4

Figure 5

Figure 6

Figure S1

Molecular Layer

Internal Granular Layer

Figure S2

A

lobe culture

merge	EGFP DAPI	GFAP	Calbindin	
				EGL
				ML
				PCL
				IGL

B

slice culture

merge	EGFP DAPI	GFAP	Calbindin	
				EGL
				ML
				PCL
				IGL